

Accepted Manuscript

Experimental and theoretical spectroscopic studies, HOMO–LUMO, NBO analyses and thione-thiol tautomerism of a new hybrid of 1,3,4-oxadiazole-thione with quinazolin-4-one

Saied M. Soliman, Mohamed Hagar, Farahate Ibid, El Sayed H. El Ashry

PII: S1386-1425(15)00082-7
DOI: <http://dx.doi.org/10.1016/j.saa.2015.01.061>
Reference: SAA 13229

To appear in: *Spectrochimica Acta Part A: Molecular and Biomolecular Spectroscopy*

Received Date: 8 September 2014
Revised Date: 4 November 2014
Accepted Date: 25 January 2015

Please cite this article as: S.M. Soliman, M. Hagar, F. Ibid, E.S.H. El Ashry, Experimental and theoretical spectroscopic studies, HOMO–LUMO, NBO analyses and thione-thiol tautomerism of a new hybrid of 1,3,4-oxadiazole-thione with quinazolin-4-one, *Spectrochimica Acta Part A: Molecular and Biomolecular Spectroscopy* (2015), doi: <http://dx.doi.org/10.1016/j.saa.2015.01.061>

This is a PDF file of an unedited manuscript that has been accepted for publication. As a service to our customers we are providing this early version of the manuscript. The manuscript will undergo copyediting, typesetting, and review of the resulting proof before it is published in its final form. Please note that during the production process errors may be discovered which could affect the content, and all legal disclaimers that apply to the journal pertain.



Experimental and Theoretical Spectroscopic Studies, HOMO–LUMO, NBO Analyses and Thione-Thiol Tautomerism of a New Hybrid of 1,3,4-Oxadiazole-thione with Quinazolin-4-one

Saied M. Soliman^a, Mohamed Hagar^b, Farahate Ibid^a, El Sayed H. El Ashry^{a*}

- a. *Chemistry Department, Faculty of Science, Alexandria University, Alexandria 21321, Egypt.*
- b. *Chemistry Department, Faculty of Science, Taibah University, Yanbu Branch, Yanbu, KSA.*

Abstract

The hybrid 3-(4-chlorophenyl)-2-[(5-thioxo-4,5-dihydro-1,3,4-oxadiazol-2-yl)methylthio]quinazolin-4(3H)-one has been synthesized and characterized using elemental analysis, FTIR and NMR spectroscopy. The thione-thiol tautomeric equilibria has been studied using both DFT/B3LYP and HF methods at different basis sets. The results of calculations showed predominance of the thione form. The molecular structure and vibrational spectra of the stable tautomer are predicted using the same level of theory. The complete assignments of the vibrational modes were performed on the basis of potential energy distribution (PED). The 6-311++G(d,p) gave the best results compared to the experimental data. The chemical shift values of the two tautomers are calculated using GIAO method. The NH proton of the thione tautomer have chemical shift value closer to the experimental data compared to the SH proton of the thiol one. The electronic transitions are predicted using the TD-DFT calculations at B3LYP/6-311++G(d,p) level of theory. The calculated polarizability and first hyperpolarizability showed that the studied compound has better NLO properties than urea. The Molecular Electrostatic Potential (MEP) analysis reveals the sites for electrophilic and nucleophilic attack in the molecule. NBO analysis is carried out to investigate the stabilization energy of various intramolecular charge transfer interactions within the studied molecule.

Key words: Oxadiazole - Quinazoline - Tautomerism - thione – NBO - NMR

Corresponding Author: E. S. H. El Ashry, Tel: +201227430924, e-mail: eelashry60@hotmail.com

Introduction

The quinazoline skeleton [1] is of a great importance to chemists as well as biologists as it is available in a large variety of naturally occurring compounds. It is also found in clinically useful molecules having diverse biological activities [2] such as antiviral, antimalarial, anticonvulsant, antibacterial, diuretic, hypnotic, hypoglycaemic, antitumoral and antihypertensive. It has been reported that substitution of different heterocyclic moieties at 2 or 3 position of quinazolinone nucleus modulates the anti-inflammatory activity. A large numbers of azetidinones, [3,4] thiazolidinones [5, 6] and oxadiazoles [7-9] were reported to possess anti-inflammatory activity.

Also, the biological activity of compound strongly depends on acid-base interactions which is an addition to behavior associated with its permeability through cell membranes and its spatial structure [10]. The geometric structure is important for determining many factors that could affect its biological activity such as atomic charge density, dipole moment, polarizability and the ability to interact with biomolecules through coordinative or hydrogen bonds as well as dipole-dipole interactions [11,12].

On other hand, the spectroscopic investigations using infrared, electronic and NMR spectroscopy are considered as the most important tools to study the molecular structure of organic compounds. From this point of view, the aim of this study is to fully determine the molecular structure, IR spectra, NMR chemical shifts, absorption wavelengths, excitation energies and dipole moment as well as nonlinear optical properties of newly prepared quinazoline-oxadiazolyl derivative. The titled compound has the two possible tautomers shown in Fig. 1a. The relative stability of the thiol (T1) and thione (T2) tautomers was reported. For computations, we have carried out HF and DFT calculations. Detailed interpretations of the vibrational spectra of our compound have been made based on the calculated potential energy distribution (PED).

2. Experimental

2.1. General

Melting points were determined on a meltemp apparatus and are uncorrected. IR spectra were recorded with a Tensor 37 Bruker infrared spectrophotometer as potassium bromide pellets and frequencies were reported in cm^{-1} . ^1H NMR and ^{13}C NMR spectra were determined with a JEOL spectrometer at 600 MHz. The chemical shifts are expressed in the δ scale using tetramethylsilane as a reference. TLC were

performed on Merck Kiesel gel; 60-F254 plates, and the spots were detected by UV light absorption.

2.2. 3-(4-chlorophenyl)-2-[(5-thioxo-4,5-dihydro-1,3,4-oxadiazol-2-yl)methylthio]quinazolin-4(3H)-one

The starting material 2-(ethoxycarbonylmethyl)thio-3-(4-chlorophenyl)-4-oxo-3*H*-quinazoline was prepared according to the reported method [13]. The treatment of this ester with hydrazine hydrate afforded the corresponding hydrazide **1** [14]. To a solution of **1** (0.5 g, 1.4 mmol) in ethanol (15 mL) was added a solution of potassium hydroxide (0.08 g, 1.4 mmol) in water (2 mL) and carbon disulphide (0.4 mL) as shown in Fig. 1. The solution was heated under reflux for 4 hr. The solvent was evaporated and the residue was dissolved in water, filtered and acidified with dilute hydrochloric acid. The precipitate was filtered off, washed with water, and recrystallized from ethanol to give dark yellow crystals; yield: 27 %; mp 135-137 °C, R_f 0.50 (1:1 EtOAc- petroleum ether).

IR (KBr, in cm^{-1}): 3462 (NH), 3088-3041 (CH, aromatic), 2922 (CH alkane), 1656 (CO).

^1H NMR (DMSO- d_6): δ 4.54 (s, 2H, H35, H36), 7.51 (ddd, $J= 1.2, 8.2, 8.0$ Hz, 1H, H27), 7.56-7.58 (m, 3H, H31, H33, H29), 7.68 (dd, $J= 3.0, 9.5$ Hz, 2H, H32, H34), 8.09 (dd, $J=1.2, 8.0$ Hz, 1H, H28), 8.86 (ddd, $J= 1.2, 8.0, 8.2$ Hz, 1H, H30), 13.1 (s, 1H, oxadiaz-H). ^{13}C NMR: δ 26.3 (C25), 120.1(C5), 126.5 (C1), 127.0 (C3), 127.1 (C6), 130.2 (C13), 132.0 (C15), 134.8 (C11), 135.5 (C14), 135.6 (C2), 147.3 (C4), 155.2 (C19), 161.0 (C10), 161.1 (C8), 178.3 (C21).

^1H NMR (CDCl_3): δ 4.44 (s, 2H, H35, H36), 7.31 (d, 2H, $J= 7.3$ Hz, H31), 7.47 (dd, 1H, $J= 6.7, 7.2$ Hz, H27), 7.55 (d, 2H, $J= 7.3$ Hz, H32), 7.65 (d, 1H, $J= 7.3$ Hz, H29), 7.79 (dd, 1H, $J= 7.2, 7.3$ Hz, H28), 8.25 (d, 1H, $J= 7.2$ Hz, H30), 11.1 (s, 1H, oxadiaz-H). ^{13}C NMR: δ 26.1 (C25), 119.8 (C5), 126.5 (C1), 126.8 (C3), 127.4 (C6), 130.3 (C13), 130.6 (C12), 133.4 (C11), 135.2 (C14), 135.5 (C2), 147.2 (C4), 153.6 (C19), 160.4 (C10), 161.6 (C8), 178.6 (C21).

^1H NMR ($\text{CD}_3\text{CN}-d_3$): δ 4.47 (s, 2H, H35, H36), 7.44 (d, 2H, $J= 8.7$ Hz, H32, H34), 7.50 (dd, 1H, $J= 7.3, 8.0$ Hz, H27), 7.62-7.64 (m, 3H, H31, H33, H29), 7.84 (dd, 1H, $J= 7.3, 8.0$ Hz, H28), 8.17 (d, 1H, $J= 7.9$ Hz, H30) 10.33 (s, 1H, oxadiaz-H).

3. Computational details

The quantum chemical calculations have been performed at HF and DFT (B3LYP) methods to predict the relative stability of the two possible tautomers of the titled compound using Gaussian 03 package [15]. The basis sets used are 6-31G(d,p), 6-311G(d,p) and 6-311++G(d,p). The optimized structural parameters have been used to calculate the vibrational frequencies at the different levels of theories. The calculations converged to the optimized geometries having true energy minima, as revealed by the lack of imaginary frequencies in the vibrational mode calculations. The assignments of the calculated normal modes have been made using PED analysis. The PEDs are computed using VEDA program [16]. The chemical shift values of the suggested tautomers are calculated using GIAO method to simulate the experimentally measured NMR spectra. Also, the electronic spectra were calculated using TD-DFT method to predict the excitation energies of the most stable tautomer.

4. Results and discussion

4.1. Tautomerism and thermodynamic Properties

The tautomerism of organic compounds has been subjected to extensive theoretical studies using various quantum-chemical approaches [17]. Oxadiazole thione ring can exist in two possible tautomeric forms; thiol and thione tautomers. A schematic representation of the two possible tautomers is shown in Fig. 1a. In the present paper, a combined experimental and theoretical spectral studies were used to show which tautomer could exist. From this point of view, we used quantum chemical calculations to predict the most stable tautomer of the studied molecule in the framework of both the HF and DFT methods using different basis sets. Table S1 (Supplementary materials) presents the theoretically computed corrected total energy (E_{corr}), Gibbs free energies (G), entropies (S) and enthalpies (H) of the studied tautomers using HF and DFT methods. It is found that; thione tautomer (T2) is the most stable form. The calculated relative energy (ΔE) and relative Gibbs free energy (ΔG) of T2 with respect to T1 are presented in the same table. The energy differences (ΔE) between these two tautomers are predicted to be in the range of 8.30-9.37 kcal/mol and 6.34-7.62 kcal/mol using DFT and HF methods, respectively. The tautomeric equilibrium constants (k) between them were calculated using the equation $K = e^{-(\Delta G/RT)}$ where the gas constant (R) is 2×10^{-3} kcal/mol.k and the temperature (T) is 298.15 k. The values of the equilibrium constant (k) for this tautomeric equilibria are used to calculate the

mole fractions of individual tautomers. The mole fractions of the tautomer T1 is almost null. So, the studied molecule exists only as thione tautomer (T2).

4.2. Molecular geometry and structural properties

The molecular structure and atom numbering of the stable tautomer (T2) are shown in Fig. 2. The optimized geometrical parameters (bond lengths and angles as well as dihedral angles) of the most stable tautomer obtained by HF and DFT/B3LYP methods with different basis sets are presented in Table S2 (Supplementary materials). The results are compared with the experimental X-Ray structure of the structurally related compound [18]. From Table S2, it is found that the bond lengths and bond angles calculated by DFT/B3LYP and HF methods are consistent with experimental values. The maximum deviations of the calculated bond distance and bond angle values from the experimental data are 0.032 Å and 3.061°, respectively, using DFT method while, 0.035 Å and 3.045° using HF method, respectively. The changes of the bond distance and bond angles due to changing the basis set do not exceed 0.005 Å and 0.547°, respectively. The calculated bond distances are found to have higher values in case of HF calculations with respect to B3LYP computations except C19–C25 and C21–S24. On other hand, some of the B3LYP calculated bond angles are overestimated while the others are underestimated compared to the HF method.

The values of the calculated dihedral angles (see Table S2) indicate that, the quinazoline, phenyl and the oxadiazole are planar rings. Also the N7–C8–S16–C25 and N9–C8–S16–C25 dihedral angles are -175.468 and 5.449° respectively indicating that, the C–S bond is slightly twisted from the quinazoline ring plane. On other hand, the plane passing through the oxadiazol ring makes an angle of 81.12° with the quinazoline ring plane. The angle between the quinazoline ring plane and p-chlorophenyl ring is 87.98°. Consequently, oxadiazole and p-chlorophenyl rings are almost perpendicular to the quinazoline ring (see Fig. 2). Furthermore, the calculations showed the presence of intramolecular hydrogen bonding interaction between H35 and N7 atoms. The calculated N...H intramolecular distance is 2.177Å and the C–H...N angle is 118.914°.

4.3. Natural Atomic Charges

The charge distribution on the molecule has an important effect on the vibrational spectra, dipole moment, polarizability, electronic structure, and more properties of molecular systems. The NPA charge distribution of T2 was calculated by HF and

B3LYP methods. From the NPA charge values listed in Table S3 (Supplementary Materials), we can observe the electropositive nature of all hydrogen atoms. The highest electropositive hydrogen is the amino group hydrogen (H37). On other hand, all the carbon atoms are electronegative except C4, C8, C10, C11, C19 and C21 as these atomic sites are bonded to strong electronegative atoms such as oxygen or nitrogen. The C8, C10, C19 and C21 atoms have higher positive charge density than the others because these carbon atoms are located between two strong electronegative atoms instead of one in the others. Of the C-atoms, the C25 and C10 have the minimum and maximum charge density, respectively. The highest electronegative atomic site in the molecule is O17. Furthermore, the charge densities at H35 and H36 atomic sites are 0.2864 and 0.2488, respectively using B3LYP/6-311++G(d,p). The higher NPA charge at the former compared to the latter is attributed to the presence of the weak non-conventional C–H35...N interaction.

4.4. Molecular electrostatic potential

Molecular electrostatic potential (MEP) is a useful quantities to illustrate the charge distributions on molecule and used to visualize variably charged regions. Since the charge distributions can give information about how the molecule interact with another one so, MEP is widely used as a reactivity map for determining sites of electrophilic and nucleophilic attack as well as in studies of biological recognition and hydrogen-bonding interactions [19–22]. To predict the reactive sites of electrophilic and nucleophilic attack for the investigated molecule, the MEP at the B3LYP/6-311++G(d,p) optimized geometry was calculated and shown in Fig. 3. Potential decreases in the order blue > green > yellow > orange > red. The negative (red) regions of the MEP are related to electrophilic reactivity, and the positive (blue) regions are related to nucleophilic reactivity. The MEP map shows that the region of maximum negative electrostatic potential is located around O17 with MEP value around -0.0497 a.u while the most positive region is localized on H37 with a value of +0.0669 a.u. So, it is expected that the most preferred region for electrophilic and nucleophilic attack is that around O17 and H37, respectively. These sites give information about the region from where the compound can make intermolecular interactions.

4.5. Vibrational analysis and theoretical prediction of spectra

The experimental and theoretical vibrational spectra of the studied compound are shown in Fig. 4. The calculated wave numbers along with their relative intensities

using HF and DFT methods at different basis sets and their assignment based on potential energy distribution (PED) are summarized in Tables S4 (Supplementary materials) and 1. The disagreements between the calculated and observed vibrational wavenumbers are attributed to neglecting the anharmonicity present in real system. Furthermore, the experiments were performed for solid samples while calculations were made for a free molecule in gas phase. The optimal scaling factors [23] are calculated at DFT and HF methods using different basis sets and their average values are presented in the same table. Generally, the DFT method gave better quantitative prediction for infrared vibrations than the HF one [24]. Since, the use of the more sophisticated basis set 6-311G++(d,p) gave better agreement with the experimental data than either the 6-31g(d,p) or 6-311G(d,p) so, PED discussion are described based on the B3LYP/6-311G++(d,p) results.

4.5.1. N–H vibrations

The stretching of the amino group of the secondary amines appeared around 3500–3000 cm^{-1} in the IR absorption spectra [25]. The band appeared experimentally at 3462 cm^{-1} is due to N–H stretching vibration which is calculated at 3672 cm^{-1} using the B3LYP/6-311G++(d,p) method. Also the N–H bending of secondary amines appeared in the range of 1580-1490 cm^{-1} . In the present work, this bending vibration is calculated at 1491 cm^{-1} . Other contributions to the NH bending vibrations are predicted at lower frequency (modes 31, 32 and 38). It is noted that these N–H bending modes are almost masked by the aromatic ring vibrations [25].

4.5.2. C–H vibrations

The studied compound has three ring systems, the 1,4-disubstituted benzene (R1), the quinazoline (R2) and the oxadiazole (R3) rings. The aromatic C–H ring stretching vibrations are normally found between 3100 and 3000 cm^{-1} [26]. In the present work, the eight C–H stretching modes are observed in the range of 3088-3041 cm^{-1} , for which the calculated wavenumbers are in the range of 3209-3171 cm^{-1} using B3LYP/6-311++G(d,p) level. The visual inspection of these modes using Gaussview software showed the four C–H stretching modes of the p-substituted benzene (R1) at 3209, 3207, 3192 and 3191 cm^{-1} while the four C–H stretching vibrations of the quinazoline ring (R2) are predicted at 3203, 3197, 3186 and 3171 cm^{-1} . The symmetric $\nu(\text{C–H})$ modes are calculated at 3209, 3207, 3203 and 3197 cm^{-1} while the asymmetric C-H stretching vibrations are predicted at 3192, 3191, 3186 and 3171 cm^{-1} .

¹. The aliphatic C–H stretching vibrations usually appear at lower frequency than the aromatic stretching modes. The aliphatic C–H stretching vibrations are observed experimentally at 2922 cm⁻¹. The asymmetric and symmetric C–H stretching vibrations of the methylene group are predicted using PED analysis at 3146 and 3058 cm⁻¹, respectively. The asymmetric vibration occurs at higher frequency and lower intensity than the symmetric one.

Also, the DFT calculations predicted the in-plane C–H bending vibrations in the range of 1590-1101 cm⁻¹ (except modes 21, 22, 25, 26, 29-32, 35-39) while the out of plane C–H deformations are predicted in the range of 1033-801cm⁻¹ (except modes 52, 53, 56, 57) and at lower frequencies of 708, 519 and 423 cm⁻¹. The out-of-plane C-H bending were used to differentiate between the position of the substituents in the disubstituted benzene (ortho, meta and para). The para disubstituted benzene derivatives are characterized by out-of-plane C-H bending mode in the range of 860-800 cm⁻¹. In the present work, these bands are observed in the range of 801-845 cm⁻¹. The bending vibrations of the aliphatic CH₂ group such as scissoring, wagging and twisting modes are predicted at 1489, 1270 and 1207 and 1155 cm⁻¹, respectively. All C–H vibrations are in good agreement with the experimental data.

4.5.3. C–O and C–S vibrations

The $\nu(\text{C}=\text{O})$ band is observed experimentally at 1656 cm⁻¹ while calculated at 1754 cm⁻¹ using the B3LYP/6-311++G(d,p) method. It is known that the C–O stretching vibrations occur at lower frequency than the $\nu(\text{C}=\text{O})$. The PED analysis predicted contribution to the $\nu(\text{C}=\text{O})$ vibration at 1358 cm⁻¹. Also, the C=S and C–S bonds showed lower absorption frequency as compared to C=O and C–O bonds, respectively, due to the decreased force constant and increase in reduced mass when oxygen atom replaced with sulphur. The C=S stretching vibration (1277 cm⁻¹) is predicted at lower frequency than $\nu(\text{C}=\text{O})$. Also, the C–S stretching vibrations (743 and 659 cm⁻¹) are predicted at lower frequency than $\nu(\text{C}=\text{O})$.

4.5.4. C–N and C–C vibrations

The ring C=N and C=C stretching vibrations occur in the region of 1600-1500 cm⁻¹ [26] and 1625-1400 cm⁻¹ [27], respectively. Almost the C=N and C=C stretching vibrations are found overlapped in the same region and difficult to be assigned. These stretching vibrations are observed at 1612 cm⁻¹. The present DFT calculations predicted the C=N stretching vibrations at 1657 and 1590 cm⁻¹, respectively, while the C=C stretching vibrations in the range of 1657-1615 cm⁻¹. The $\nu(\text{C}=\text{N})$ modes

calculated at 1657 and 1590 cm^{-1} are due to the C19=N23 (R3) and C8=N7 (R2) stretching vibrations, respectively. It is well known that, the C–N stretching vibrations are usually occur at lower frequency (1300-1200 cm^{-1}) than the C=N stretching vibrations [28]. The C–N stretching vibrations are predicted at 1358, 1310, 1277 and 1217 cm^{-1} (exp. 1302 and 1209 cm^{-1}).

4.5.5. Other vibrations

The C–Cl stretching band is normally expected around 750–580 cm^{-1} [29]. Two contributions to the stretching vibrations of the C–Cl bond are predicted at 615 and 449 cm^{-1} . The $\nu(\text{N–N})$ of the oxadiazole ring is predicted using the B3LYP/6-311++G(d,p) method at 1067 cm^{-1} while experimentally observed at 1064 cm^{-1} .

4.6. Electronic spectra and HOMO–LUMO analysis

The molecular orbital (MO) calculations indicated that the title compound has 103 occupied molecular orbitals (MOs). The highest one in energy is called the highest occupied molecular orbital (HOMO) while LUMO refers to the lowest unoccupied molecular orbital (LUMO). The energy values of the HOMO and LUMO levels indicate the reactivity of molecule as donor and acceptor of electrons, respectively. Also, HOMO and LUMO energies are considered as important parameters in determining molecular properties [30]. The difference in energy between HOMO and LUMO is called the excitation energy which indicates the chemical reactivity of the molecule towards electron transport and recently used to establish the bioactivity from intramolecular charge transfer [31,32]. The E_{HOMO} , E_{LUMO} and ΔE are calculated to be -6.5300, -1.8044 and 4.7256 eV, respectively.

In order to get the accurate description of the electronic transitions, the first 20 spin allowed singlet-singlet excitations were calculated using the TD-DFT method. Of these transitions, only those of the highest oscillator strength are discussed. The results are shown in Table S5 (Supplementary materials) which represents the calculated λ_{max} values with their major contributions of molecular orbitals to the predicted electronic transitions. The highest wavelength band is calculated at 294.9nm which corresponds to the transition from the HOMO and HOMO-2 to LUMO. The frontier molecular orbital (FMO) plot drawn by DFT-B3LYP method using 6-311++G(d,p) basis set is shown in Fig. 5. It can be seen that the electron densities of the ground state MOs are mainly localized on the π -system and the lone pair of S-atoms so; the electronic transition from the ground state to the excited state is predicted to be mixed π - π^* and n - π^* transitions.

4.7. NMR

The isotropic magnetic shielding (IMS) values calculated using the GIAO approach at the 6-311++G(d,p) level are used to predict the ^{13}C and ^1H chemical shifts (δ_{calc}) for the studied tautomers and the results are compared with the experimental NMR data (δ_{exp}) as shown in Table 2. The calculated chemical shift values are in good agreement with the experimental data except H37. This large difference between the calculated and experimental chemical shift value for H37 is attributed to the high polarity of the N–H bond. In solution, this group undergoes strong solute-solvent interactions especially with polar solvents such as DMSO which is not the case in the gas phase. Moreover, the chemical shift of the H37 in the less polar CDCl_3 solvent is found closer to the calculated value than that in DMSO. This indicates that, the deviation of the calculated chemical shift value for the H37 proton from the experimental data is mainly attributed to the medium effect. Moreover, correlation graphs between the calculated and experimental ^1H -NMR chemical shifts for the T2 tautomer is shown in Fig. S1 (Supplementary Material). It can be seen that H35 proton deviate significantly from the straight line relation obtained which is probably due to the intramolecular C–H35...N interaction. Such interaction is not important in presence of solvent as the intermolecular solute-solvent interactions become more important in solution. From this point of view, omitting this point from the correlation gave the ^1H -NMR correlation graphs shown in Fig. S2 (Supplementary Material). The correlation coefficient for the T2 ($R^2=0.974$) tautomer is better than the T1 ($R^2=0.940$). Also, the correlation graphs between the calculated and experimental ^{13}C -NMR chemical shifts for the studied tautomers are shown in Fig. S3 (Supplementary Material). The correlation equations are

$$y = 1.315x - 2.622 \quad R^2 = 0.940 \quad \text{T1 } (^1\text{H-NMR})$$

$$y = 0.799x + 1.609 \quad R^2 = 0.975 \quad \text{T2 } (^1\text{H-NMR})$$

$$y = 0.994x - 6.205 \quad R^2 = 0.970 \quad \text{T1 } (^{13}\text{C -NMR})$$

$$y = 0.973x - 4.250 \quad R^2 = 0.987 \quad \text{T2 } (^{13}\text{C -NMR})$$

The correlation coefficients are better for the T2 tautomer than the T1 one.

4.8. NLO properties

The development of materials with large nonlinear optical (NLO) properties has been of great interest in past few decades. These materials find numerous device applications, from lasers to optical switches and electronics [33]. So far, the organic π -conjugated molecules have been considered mostly for this purpose because of their

easy functionalization to fine tune the desired properties and the ease of fabrication and integration into devices [34-36]. NLO is very important in areas such as telecommunications, optical interconnections and signal processing [37, 38].

The components of the dipole moments μ (Debye), static polarizability components α (a.u.), the average polarizability (or linear polarizability) α_0 (\AA^3), and the first hyperpolarizability components β (a.u.), the first hyperpolarizability β_0 ($\times 10^{-31} \text{ cm}^5 \text{ esu}^{-1}$) of the studied compound are given in Table 3. The μ , α_0 and β_0 are calculated to be 5.066 Debye, 39.39\AA^3 and $11.52 \times 10^{-31} \text{ cm}^5 \text{ esu}^{-1}$, respectively. These are important parameters in discussions of the NLO of a molecule. The α_0 and β_0 values of the title compound are about 8 and 9 times, respectively greater than those of urea ($\alpha_0=4.28 \text{\AA}^3$, $\beta_0=1.52 \times 10^{-31} \text{ cm}^5 \cdot \text{esu}^{-1}$) which is considered as important molecule used in the comparative purposes of the NLO properties of molecular systems. Also, the NLO properties of a molecule are related to the energy gap between HOMO and LUMO. The B3LYP/6-311++G(d,p) calculated energy gap is 4.7256 eV which is lower than urea ($\Delta E= 6.7063 \text{ eV}$). Thus, the studied compound can be regarded as a good applicant for NLO materials.

4.9. Natural Bond Orbital Analysis

Natural Bond Orbital (NBO) analysis presents an efficient method for studying interesting features of molecular structure. It gives a strong insight in the intra and intermolecular bonding and interaction among bonds. Also, it provides a convenient basis for investigating charge transfer in molecular system [39]. Table S6 (Supplementary materials) gives the occupancy of electrons and p-character in the significant NBOs [40]. For C-H bonds, all the hydrogen atoms have almost 0% of p-character. On contrary, 100% p-character was observed in both the atoms in π -bonding of the C-C, C-N and C-O bonds. It is noted that, the LP of N9 and N22 atoms having 100% p-character while the LP of N7 and N23 has 72.97 and 59.91 % p-character. Also, LP(1) of Cl26, S24, S16, O17 and O20 have 17.34, 18.55, 29.96, 41.07 and 60.92 % p-character, respectively, while almost 100% p-character was observed in the LP(2) of these atoms as well as LP(3) of Cl26. The coefficients C8(0.61)-N9(0.79) and C19(0.56)-O20(0.83) are called polarization coefficients. The magnitude of these coefficients shows the importance of the two hybrids in the formation of the bond. It is clear that, both nitrogen and oxygen have larger percentage of NBO and give the larger polarization coefficients than carbon because these atoms have the higher electronegativity.

Another useful aspect of NBO method is that it gives information about interactions in both filled and virtual orbital spaces that could enhance the analysis of intra and intermolecular interactions. Delocalization of the electron density between occupied NBO (bond (or) lone pair) and the unoccupied NBO corresponding to a stabilizing donor–acceptor interactions. The energy of this interaction can be estimated by the second order perturbation theory [41]. Table 4 lists the calculated second order interaction energies ($E^{(2)}$) between the donor–acceptor orbital's in the titled molecule. The larger the $E^{(2)}$ value, the intensive is the interaction between electron donors and electron acceptors, i.e., the greater the extent of conjugation of the system.

The delocalization of electrons due to $LP(1)N9 \rightarrow BD^*(2)N7-C8$, $LP(1)N9 \rightarrow BD^*(2)C10-O17$ and $LP(1)N22 \rightarrow BD^*(1)C21-S24$ having the highest intramolecular charge transfer interaction (ICT) energies ($E^{(2)}$) of 53.25, 43.28 and 71.58 kcal/mol respectively. Moreover, the interactions $BD(2)C-C \rightarrow BD^*(2)C-C$, $BD(2)C-C \rightarrow BD^*(2)N-C$, $BD(2)N-C \rightarrow BD^*(2)C-C$ and $BD(2)C-C \rightarrow BD^*(2)C-O$ are responsible for conjugation of the ring π -bonds indicate strong π -electron delocalization within ring leading to a maximum stabilization of energy upto 25.17 kcal/mol. The movement of π -electron cloud from donor to acceptor i.e. intramolecular charge transfer can make the molecule more polarized and the ICT must be responsible for the NLO properties of molecule. Therefore, the titled compound may be used for nonlinear optical materials application in future. Furthermore, the small interaction energy ($E^{(2)}=3.21$ kcal/mol) due to the ICT between $LP(1)N7$ and $BD^*(1)C25-H35$ indicates the presence of weak C–H...N intramolecular H-bonding interaction.

Conclusion

A quinazoline containing mercapto-oxadiazole is synthesized and characterized by a combined experimental and theoretical quantum chemical calculations. The DFT and HF methods using different basis sets predicted the higher stability of thione tautomer. The calculated NMR chemical shifts using GIAO method correlated well with the experimental data for thione tautomer T2 than thiol one (T1). The optimized molecular structure and spectral properties of the stable tautomer have been calculated. The theoretical vibrational spectra calculated using the 6-311G++(d,p) basis set gave better agreement with the experimental data than the other basis sets. The assignments of all the fundamental vibrational modes of the title compound were

made based on the results of the PED calculations. The calculated electronic spectra using TD-DFT predicted the longest wavelength band at 294.9nm which corresponds to the transition from the HOMO and HOMO-2 to LUMO. The dipole moments, linear polarizability and the first hyperpolarizability β_0 predicted that the studied compound has higher NLO than urea. Various intramolecular interactions that is responsible for the stabilization of the molecule was revealed by natural bond orbital analysis. The presence of C-H...N intramolecular H-bonding interaction is confirmed using the second order perturbation theory. The NPA analysis reveals the charge distribution among the atoms. The MEP analysis showed that O17 and H37 are the most preferred sites for electrophilic and nucleophilic attack, respectively.

References

- [1] D. J. Brown, Quinazolines, Supplement I; The Chemistry of Heterocyclic Compounds,; John Wiley & Sons: Chichester.55, 1996.
- [2] (a) T. Hisano, Org. Prep. Proced. Int., 5 (1973) 145–193. (b) G.Stevens, Diuretics, Academic Press Inc.: New York, 12. 1963 (c) H. J. Hess, T. H.Cronin, A.Sciabine, J. Med. Chem. 11 (1968) 130–136. (d) G. Leszkuvszky, I. Erdely, L. Tardos, Acta. Physiol. Acad. Sci. Hung. 27 (1965) 81–90. (e) C. M. Gupta, S. T. Husain, A. P.Bhaduri, N. M.Khana, S. K. Mukherjee, Nature 223 (1969) 524-525.
- [3] R. Agarwal, C. Agarwal, C. Singh, V.S. Mishra, Ind. J. Chem. 28B (1989) 893–896.
- [4] S.K. Srivastava, S.L. Srivastava, S.D. Srivastava, Ind. J. Chem. 39B (2000) 464–467.
- [5] S.K. Srivastava, R. Yadav, S.D. Srivastava, Ind. J. Chem. 42B (2004) 399–405.
- [6] (a)S. Mishra, S.K. Srivastava, S.D. Srivastava, Ind. J. Chem. 36B (1997) 826–830. (b) A. Mohmmad, A. Oberoi, A. Shah, Ind. J. Chem. 38B (1999) 237–239.
- [7] F.A. Omar, N.M. Mahfouz, M.A. Rahman, Eur. J. Med. Chem. 31 (10) (1996) 819–825.
- [8] L.V.G. Nargund, G.R.N. Reddy, V. Hariprasad, J. Pharm. Sci. 83 (1994) 246–248.
- [9] B.R. Rani, U. T. Bhalerau, M.F. Rahman, Ind. J. Chem. 29B (1990) 995–998.
- [10] W. L. F. Armarego, Fused Pyrimidines: Part I–Quinazolines; Interscience Publishers: New York–London–Sydney, 1967.
- [11]N. C. Kasuga, K. Sekino, M. Ishikawa, A. Honda, M. Yokoyama, S. Nakano, Shimada, C. Koumo, K. Nomiya, J. Inorg. Biochem. 96 (2003) 298–310.
- [12] C. X. Zhang, S. J. Lippard, Cur. Opin. Chem. Biol. 7 (2003) 481–489.
- [13] Fatmah A. M. Al–Omary, Laila A. Abou–zeid, Mahmoud N. Nagi, El–Sayed E. Habib, Alaa A.–M. Abdel–Aziz, A. S. El–Azab, S. G. Abdel–Hamide, M. A. Al–Omar, A. M. Al–Obaid, H. I. El–Subbagh, Bioorg. Med. Chem. 18 (2010) 2849–2863.
- [14] A. S. El–Azab, Phosphorus, Sulfur and Silicon 182 (2007) 333–348.

- [15] (a) M. J. Frisch, et al., Gaussian–03, Revision C.01, Gaussian, Inc., Wallingford, CT, 2004. (b) GaussView, Version 4.1, R. Dennington II, T. Keith, J. Millam, Semichem Inc., Shawnee Mission, KS, 2007.
- [16] M. H. Jamroz, Vibrational Energy Distribution Analysis VEDA 4, Warsaw, 2004–2010.
- [17] J. S. Kwiatkowski, T. J. Zielenski, R. Rein, *Adv. Quant. Chem.* 18 (1986), 85–130
- [18] S. R. Hall, F. H. Allen and I. D. Brown, *Acta. Cryst.* A47, (1991), 655–685.
- [19] P. Politzer, K.C. Daiker, *The Force Concept in Chemistry*, Van Nostrand Reinhold Co., 1981.
- [20] P. Politzer, P.R. Laurence, K. Jayasuriya, J. McKinney, *Health Perspect.* 61 (1985) 191–202.
- [21] J.S. Politzer, Murray, in: D.L. Protein, R. Beveridge, Lavery (Eds.), *Theoretical Biochemistry and Molecular Biophysics: A Comprehensive Survey*, vol. 2, Adenine Press, Schenectady, NY, 1991.
- [22] E. Scrocco, J. Tomasi, *Topics in Current Chemistry*, Springer–Verlag, Berlin, 42, 1973.
- [23] A. Destexhe, J. Smets, L. Adamowicz, G. Maes, *J. Phys. Chem.* 98 (1994) 1506–1514.
- [24] A.P. Scott, L. Radom, *J. Phys. Chem.* 100 (1996) 16502–16513.
- [25] G. Socrates, *Infrared and Raman Characteristic Group Frequencies, Tables and Charts* (third ed.) Wiley, Chichester 2001.
- [26] G. Varsanyi, *Assignments for Vibrational Spectra of Seven Hundred Benzene Derivations*, vol. 1, Adam Hilger, London, 1974.
- [27] V. Krishnakumar, N. Surumbarkuzhali, S. Muthunatesan, *Spectrochim. Acta Part A* 71 (2009) 1810–1813.
- [28] J.B. Lambert, H.F. Shurvell, D.A. Lightner, R.G. Cooks, *Org. Struct. Spect.* Simon & Schuster/A Viacom Company, New Jersey, 1998.
- [29] C. S. Hiremath and T. Sundius, *Spectrochim. Acta Part A*, 74 (2009) 1260–1267.
- [30] M. Amalanathan, V.K. Rastogi, I.H. Joe, M.A. Palafox, R. Tomar, *Spectrochim. Acta A* 78 (2011) 1437–1444.
- [31] L. Padmaja, C. Ravi Kumar, D. Sajan, I.H. Joe, V.S. Jayakumar, G.R. Pettit, *J. Raman Spect.* 40 (2009) 419–428.

- [32] S. Sagdinc, H. Pir, *Spectrochim. Acta A73* (2009) 181–187.
- [33] P. N. Prasad, D. J. Williams *Introduction to nonlinear optical effects in molecules and polymers* (New York: Wiley) 1991.
- [34] G. A. Lindsay, K. D. Singer (eds) *Polymers for second-order nonlinear optics*, ACS Symposium Series, No. 601 (Washington, DC: ACS) 1995.
- [35] D. M. Burland (ed.) *Chem. Rev.* 94 (1994) 1–2.
- [36] E. Hanamura, *Phys. Rev. B* 37 (1988) 1273–1279.
- [37] V. M. Geskin, C. Lambert, J. L. Bredas, *J. Am. Chem. Soc.* 125 (2003) 15651–15658.
- [38] D. Sajan, H. Joe, V.S. Jayakumar, J. Zaleski, *J. Mol. Struct.* 785 (2006) 43–53.
- [39] F. Weinhold, C.R. Landis, *Chem. Ed: Res & Pract* 2 (CERP; special “structural concepts” issue) (2001) 91–104.
- [40] A.E. Reed, L.A. Curtiss, F. Weinhold, *Chem. Rev.* 88 (1988) 899–926.
- [41] J. Chocholousova, V. Spirko, P. Hobza, *J. Phys. Chem. Chem. Phys.* 6 (2004) 37–41.

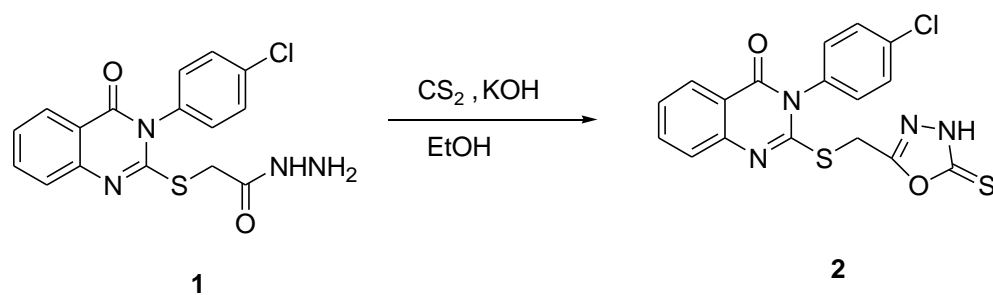


Fig. 1 The synthesis of the target compound 2.

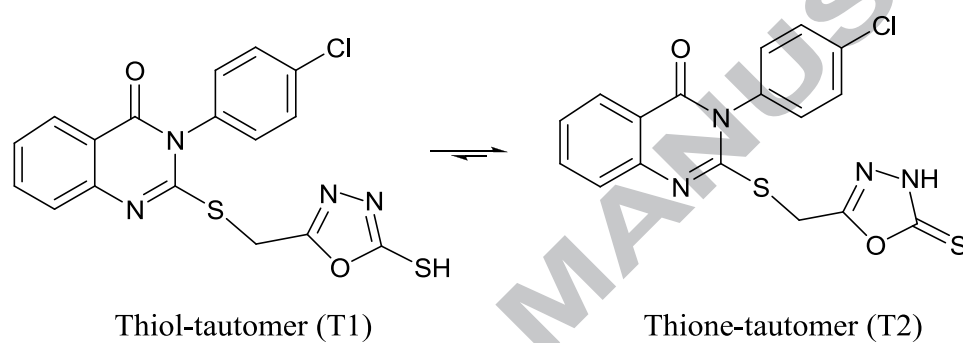


Fig. 1a. The structure of the two possible tautomers of compound 2.

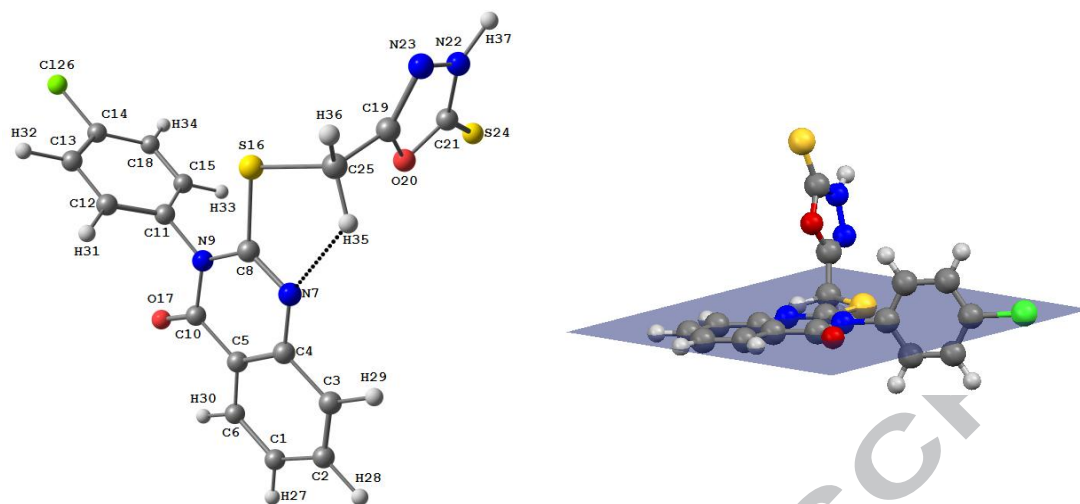


Fig. 2 The optimized molecular geometry and atom numbering scheme of the thione tautomer of compound 2.

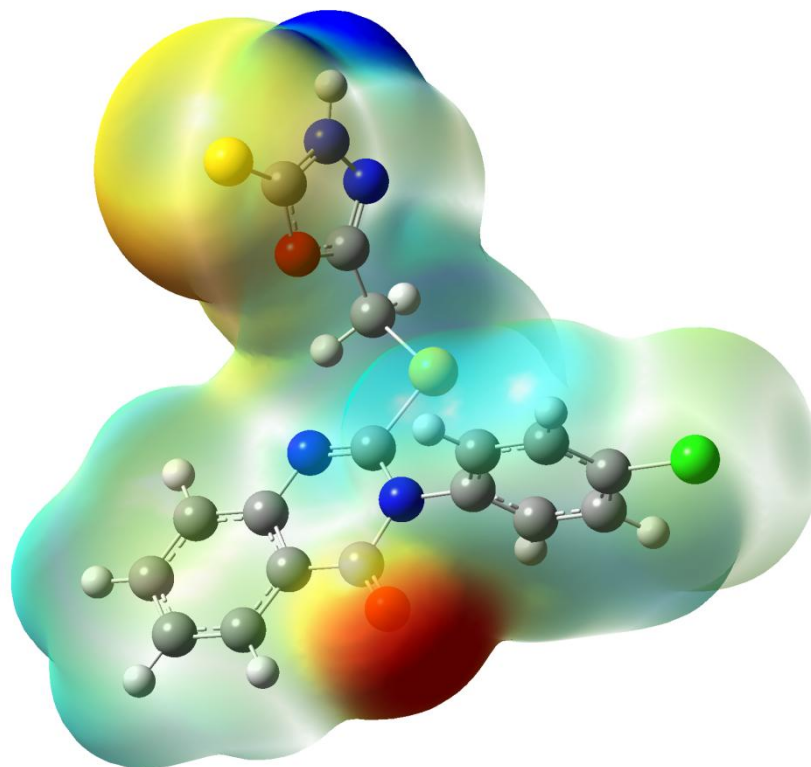


Fig. 3 Molecular Electrostatic potentials (MEP) mapped on the electron density surface calculated by the DFT/B3LYP method.

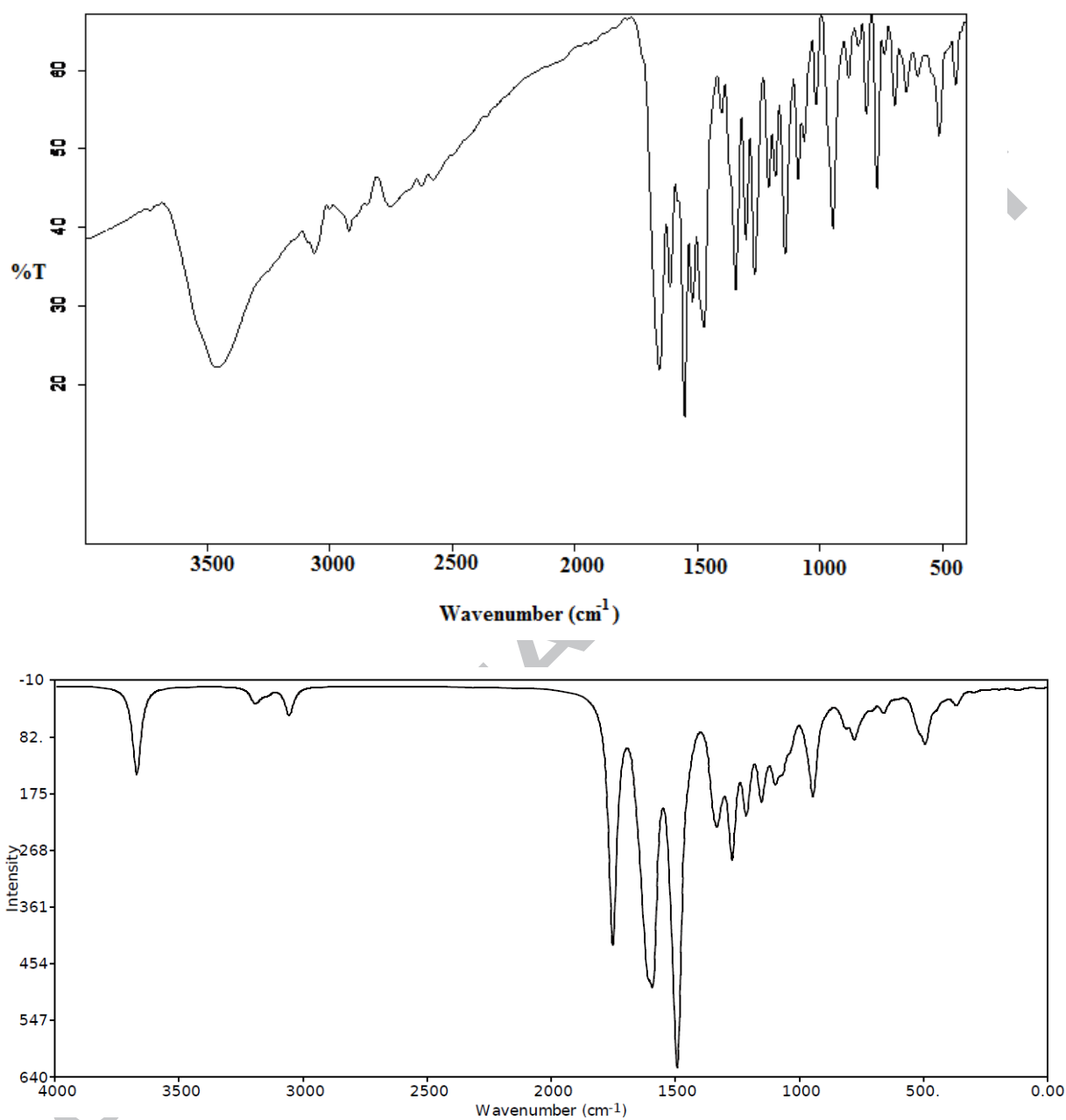


Fig. 4 The experimental (upper) and calculated (lower) vibrational spectra of compound 2.

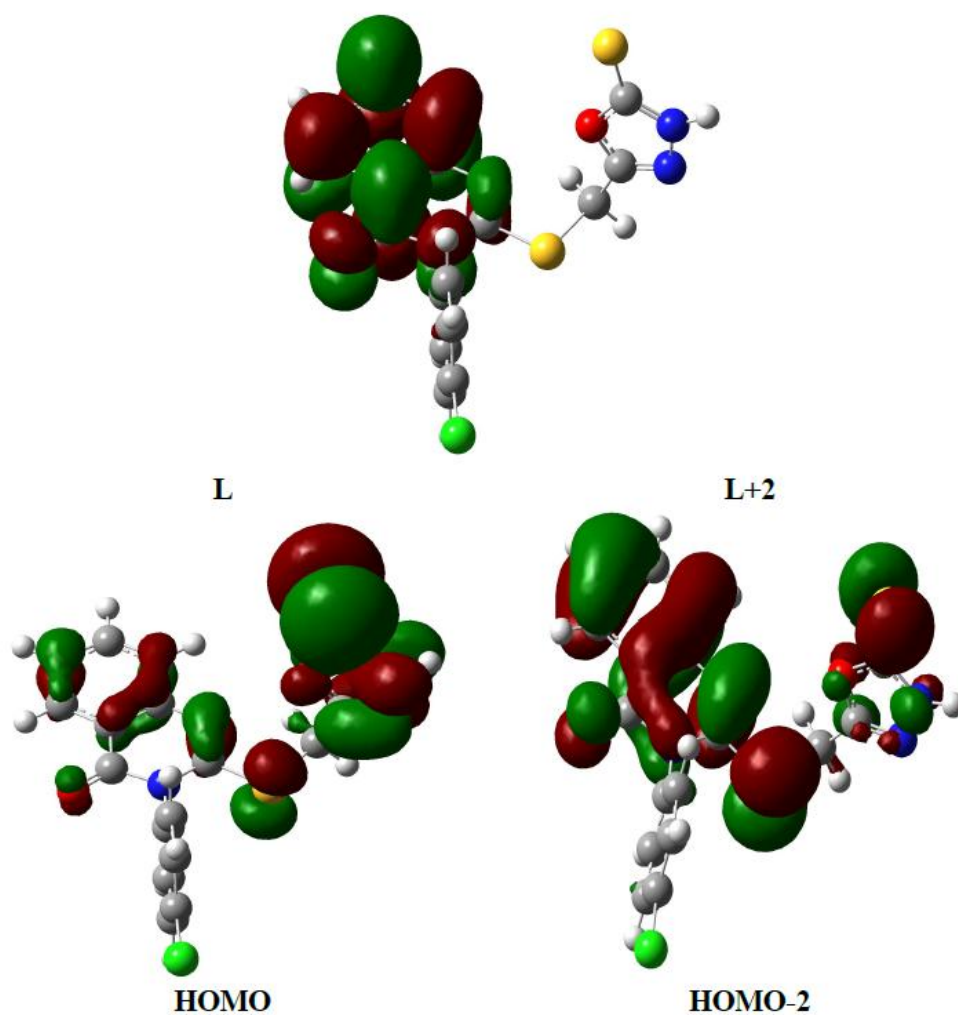


Fig. 5 The ground state isodensity surface plots for the molecular orbitals (MOs) contributed in the electronic transitions of the most stable tautomer (T2) using B3LYP/6-311++G(d,p) method.

Table 1 The Calculated vibrational frequencies (ν) in cm^{-1} and vibrational intensities (A) in kmol^{-1} for the studied compound using B3LYP method.

No.	6-31g(d,p)			6-31g(d,p)			6-31g++(d,p)			Exp.	Approximate assignment
	ν	A	S.F	ν	A	S.F	ν	A	S.F		
1	3692	139.5	0.9378	3675	143.1	0.9422	3672	144.8	0.9429	3462	100 ν_{NH}
2	3230	0.1	0.9561	3212	0.1	0.9615	3209	0.0	0.9624	3088	95 ν_{CH}
3	3228	1.3		3210	1.1		3207	0.7			97 ν_{CH}
4	3223	10.4	0.9509	3204	10.5	0.9566	3203	9.5	0.9569	3065	90 ν_{CH}
5	3217	7.4		3199	6.6		3197	5.3			86 ν_{CH}
6	3213	1.3	0.9464	3195	1.2	0.9517	3192	0.6	0.9528	3041	90 ν_{CH}
7	3211	3.1		3193	3.0		3191	3.1			89 ν_{CH}
8	3205	11.8		3187	10.7		3186	8.1			83 ν_{CH}
9	3190	4.6		3172	4.2		3171	3.7			96 ν_{CH}
10	3165	9.1		3150	7.2		3146	8.9			(15 $\nu_{\text{C25H35}}+84\nu_{\text{C25H36}}$) _{assym}
11	3071	44.4	0.9515	3065	33.0	0.9533	3058	46.9	0.9557	2922	(15 $\nu_{\text{C25H36}}+84\nu_{\text{C25H35}}$) _{sym}
12	1790	325.0	0.9251	1772	356.4	0.9347	1754	403.7	0.9444	1656	80 $\nu_{\text{C-O}}+10\delta_{\text{CNC}}$
13	1670	41.8		1661	49.5		1657	47.9			72 $\nu_{\text{C-N}}+11\nu_{\text{CC}}$
14	1663	22.8		1650	19.3		1647	26.0			51 ν_{CC}
15	1650	107.1		1636	126.9		1634	109.6			28 ν_{CC}
16	1631	259.4		1619	249.4		1616	2.8			48 $\nu_{\text{CC}}+10\delta_{\text{CNN}}$
17	1630	1.6	0.9892	1619	0.8	0.9958	1615	238.0	0.9984	1612	48 ν_{CC}
18	1609	277.0	0.9653	1594	284.3	0.9740	1590	319.9	0.9767	1553	33 $\nu_{\text{C-NCC}}+15\delta_{\text{CCC}}+15\delta_{\text{HCC}}$
19	1532	95.3	0.9931	1521	102.4	0.9998	1519	101.5	1.0010	1521	61 δ_{HCC}
20	1514	173.8		1503	206.6		1501	181.0			37 $\delta_{\text{HCC}}+10\delta_{\text{CCC}}$
21	1504	374.2		1494	361.6		1491	389.9			53 δ_{HNN}
22	1502	3.4	0.9816	1492	2.1	0.9882	1489	5.5	0.9897	1474	49 $\delta_{\text{HCH}}+42\tau_{\text{HCSC}}$
23	1453	30.9		1441	35.7		1447	27.9			41 $\nu_{\text{CC}}+10\delta_{\text{HCC}}$
24	1440	5.1	0.9733	1431	6.0	0.9795	1429	5.2	0.9810	1402	60 $\nu_{\text{CC}}+10\delta_{\text{HCC}}$
25	1376	33.4		1359	29.2		1358	26.4			10 $\nu_{\text{C-N}}+17\nu_{\text{C-O}}+22\nu_{\text{CC}}+14\delta_{\text{CCN}}$
26	1362	60.3	0.9876	1353	69.7	0.9937	1347	79.4	0.9985	1345	48 $\nu_{\text{CC}}+12\delta_{\text{CNC}}$
27	1346	108.5		1335	99.6		1331	103.2			37 $\nu_{\text{CC}}+11\delta_{\text{HCC}}$
28	1335	3.4		1323	0.2		1320	0.1			10 $\nu_{\text{CC}}+81\delta_{\text{HCC}}$
29	1323	0.2		1315	5.3		1314	5.0			82 ν_{CC}
30	1317	29.6	0.9888	1312	30.7	0.9927	1310	31.6	0.9936	1302	41 $\nu_{\text{C-N}}$
31	1286	103.8		1279	106.1		1277	103.6			13 $\nu_{\text{C-N}}+25\nu_{\text{C-S}}+30\delta_{\text{HNN}}$
32	1279	44.5		1278	19.8		1270	114.4			30 $\delta_{\text{HNN}}+30\delta_{\text{HCH}}+14\tau_{\text{HCSC}}$
33	1276	45.8	0.9931	1273	96.6	0.9953	1269	13.5	0.9981	1267	17 $\delta_{\text{CCC}}+17\delta_{\text{HCC}}$
34	1240	9.1		1232	2.4		1230	3.0			46 δ_{HCC}
35	1229	111.5	0.9835	1219	119.8	0.9917	1217	125.6	0.9936	1209	25 $\nu_{\text{C-N}}+13\delta_{\text{HCS}}$
36	1219	29.4		1217	28.3		1207	28.8			14 $\delta_{\text{HCH}}+21\delta_{\text{HCS}}$
37	1199	4.4	0.9858	1195	5.3	0.9890	1194	5.6	0.9901	1182	56 δ_{HCS}
38	1178	1.7		1171	2.7		1171	3.2			52 $\delta_{\text{HNN}}+13\delta_{\text{HCS}}+10\tau_{\text{HCSC}}$
39	1165	129.2	0.9805	1159	127.7	0.9850	1155	128.1	0.9889	1142	17 $\nu_{\text{CC}}+45\delta_{\text{HCH}}$
40	1136	15.5		1132	18.4		1132	17.9			29 $\nu_{\text{CC}}+65\delta_{\text{HCC}}$
41	1131	5.0		1127	5.0		1126	5.8			11 $\nu_{\text{CC}}+11\delta_{\text{CCC}}+20\delta_{\text{HCC}}$
42	1108	85.5	0.9835	1101	90.5	0.9901	1101	88.1	0.9903	1090	23 $\nu_{\text{CC}}+13\delta_{\text{HCC}}$
43	1088	13.8		1082	19.9		1082	21.6			21 $\nu_{\text{CC}}+10\nu_{\text{CN}}$
44	1079	74.0	0.9857	1069	70.1	0.9953	1067	63.4	0.9969	1064	54 ν_{NN}
45	1049	15.0		1044	20.7		1043	20.8			77 δ_{CCC}
46	1032	35.8	0.9841	1033	37.6	0.9835	1033	34.5	0.9840	1016	71 τ_{HCCC}
47	1004	0.0		1011	0.0		1004	0.1			31 $\delta_{\text{OCN}}+25\tau_{\text{HCCC}}$
48	990	3.3		989	3.2		986	3.4			16 $\delta_{\text{OCN}}+42\tau_{\text{HCCC}}$
49	981	0.9		988	1.2		985	1.2			42 $\tau_{\text{HCCC}}+10\tau_{\text{CCCC}}$
50	973	31.0		979	1.7		980	0.3			40 τ_{HCCC}
51	968	2.4		974	24.0		972	29.0			13 τ_{HCCC}
52	964	109.6	0.9831	961	10.0	0.9864	959	5.5	0.9885	948	32 $\delta_{\text{OCN}}+22\delta_{\text{CNN}}$
53	960	11.0		951	137.7		946	149.1			14 δ_{CNN}
54	900	9.4		901	9.8		899	8.6			54 τ_{HCCC}
55	897	0.8	0.9854	901	2.1	0.9817	889	0.9	0.9942	884	15 $\delta_{\text{CCC}}+11\tau_{\text{HCCC}}$
56	880	3.6		877	4.3		876	4.5			21 τ_{HCSC}
57	849	3.0	0.9952	848	3.7	0.9966	847	4.7	0.9971	845	32 τ_{HCCC}
58	834	0.1		832	0.0		830	0.3			84 τ_{HCCC}
59	821	35.7	0.9880	818	37.2	0.9911	818	38.6	0.9916	811	12 τ_{HCCC}
60	799	2.6		815	0.5		801	1.3			62 τ_{HCCC}
61	786	42.4	0.9773	789	53.4	0.9739	782	57.1	0.9827	768	28 $\tau_{\text{CCCC}}+37\tau_{\text{ONCC(OUT)}}$
62	766	12.7		768	10.1		765	11.0			27 $\nu_{\text{CC}}+14\delta_{\text{CNN}}+11\delta_{\text{OCN}}+10\tau_{\text{OCNN}}$
63	750	7.2		750	7.9		749	8.8			13 δ_{CCC}
64	746	6.4	0.9886	745	7.5	0.9892	743	8.0	0.9925	737	34 $\nu_{\text{C-S}}+10\tau_{\text{OCNN}}+17\tau_{\text{CONC(OUT)}}$
65	719	6.0		727	3.3		725	4.8			60 τ_{CCCC}
66	704	13.4	0.9870	710	18.4	0.9787	708	16.6	0.9823	695	11 $\tau_{\text{HCCC}}+48\tau_{\text{CCCC}}+28\tau_{\text{CONC(OUT)}}$
67	670	4.2		670	6.1		665	10.4			22 $\tau_{\text{CNCC}}+52\tau_{\text{SNOC(OUT)}}$
68	662	13.9		664	14.4		663	14.8			15 $\tau_{\text{CNCC}}+25\tau_{\text{NNSC(OUT)}}$

Table 2 A comparison of calculated chemical shifts δ (ppm) using GIAO method with experimental values in DMSO and CDCl_3 of the studied compound.

Atom	δ_{calc} (ppm)		$\delta_{\text{exp.}}$ (ppm)DMSO	$\delta_{\text{exp.}}$ (ppm) CDCl_3
	NH tautomer	SH tautomer		
C1	131.8	131.7	126.0	126.5
C2	141.5	141.3	135.6	135.5
C3	132.3	132.5	127.0	126.8
C4	154.2	154.5	147.3	147.2
C5	126.1	126.4	120.1	119.8
C6	134.5	134.5	127.1	127.4
C8	165.1	166.2	161.1	161.6
C10	167.2	167.0	161.0	160.4
C11	142.8	142.6	134.8	133.4
C12	139.0	138.9	132.0	130.6
C13	135.7	135.7	130.2	130.3
C14	153.5	154.0	135.5	135.2
C15	139.4	139.4	132.0	130.6
C18	136.4	136.2	130.2	130.3
C19	169.1	173.7	155.2	153.3
C21	187.8	171.3	178.3	178.6
C25	33.2	33.2	26.3	26.1
H27	7.6	7.62	7.51	7.47
H28	7.9	7.94	8.09	7.79
H29	7.9	7.87	7.58	7.65
H30	8.6	8.63	8.86	8.25
H31	7.4	7.33	7.56	7.31
H32	7.6	7.61	7.68	7.55
H33	7.4	7.34	7.56	7.31
H34	7.7	7.63	7.68	7.55
H35	5.7	5.6	4.54	4.44
H36	3.6	3.9	4.54	4.44
H37	8.2	4.8	13.1	11.1

Table 3 The dipole moments components μ (D), static polarizability components (a.u.), the average polarizability α_0 (\AA^3) and the first hyperpolarizability components β (a.u.) and the first hyperpolarizability β_0 ($\times 10^{-31}$ cm⁵ esu⁻¹) of T2.

μ_x	1.0826	β_{xyy}	94.8318
μ_y	-0.3000	β_{yyy}	-122.5307
μ_z	-4.9401	β_{xxz}	-52.9993
μ_{tot}	5.0662	β_{xyz}	192.6732
α_{xx}	304.0894	β_{yyz}	-107.0218
α_{xy}	34.9806	β_{xzz}	33.3502
α_{yy}	277.3650	β_{yzz}	59.2135
α_{xz}	3.3166	β_{zzz}	-3.5027
α_{yz}	13.0512	β_{xyy}	41.9132
α_{zz}	215.9849	β_{yyy}	-61.1724
α_0	39.3894	β_x	1469.1743
		β_y	4440.8551
		β_z	11876.7916
		β_0	11.5220

Table 4 The second order perturbation energies $E^{(2)}$ (kcal/mol) of the most important charge transfer interactions (donor–acceptor) in the studied compound using B3LYP/6-311++G(d,p) method.

Donor NBO (i)	Acceptor NBO (j)	$E^{(2)}$ ^a kcal/mol	$E(j)-E(i)$ ^b a.u.	$F(i,j)$ ^c a.u.
BD(2)C1-C6	BD*(2)C2-C3	20.37	0.29	0.069
BD(2)C1-C6	BD*(2)C4-C5	17.59	0.28	0.064
BD(2)C2-C3	BD*(2)C1-C6	16.77	0.29	0.063
	BD*(2)C4-C5	21.2	0.28	0.071
BD(2)C4-C5	BD*(2)C1-C6	19.46	0.29	0.07
	BD*(2)C2-C3	14.82	0.29	0.06
	BD*(2)N7-C8	11.32	0.25	0.048
	BD*(2)C10-O17	25.71	0.27	0.076
BD(2)N7-C8	BD*(2)C4-C5	16.27	0.37	0.075
BD(2)C11-C12	BD*(2)C13-C14	19.09	0.28	0.066
	BD*(2)C15-C18	21.28	0.29	0.071
BD(2)C13-C14	BD*(2)C11-C12	20.37	0.29	0.07
	BD*(2)C15-C18	18.48	0.3	0.067
BD(2)C15-C18	BD*(2)C11-C12	20.27	0.28	0.067
	BD*(2)C13-C14	22.13	0.27	0.07
LP(1)N7	BD*(1)C4-C5	8.05	0.91	0.078
	BD*(1)C8-N9	15.18	0.76	0.097
	BD*(1)C25-H35	3.21	0.74	0.045
LP(1)N9	BD*(2)N7-C8	53.25	0.27	0.108
	BD*(2)C10-O17	43.28	0.29	0.102
LP (1)S16	BD*(1) N7-C8	4.12	1.25	0.064
LP(2)S16	BD*(2)N7-C8	23.91	0.25	0.072
LP(2)O17	BD*(1)C5-C10	17.24	0.71	0.101
	BD*(1)N9-C10	31.78	0.62	0.126
LP (1)O20	BD*(1)C19 -N23	4.5	1.16	0.065
LP(2)O20	BD*(2)C19-N23	35.26	0.34	0.099
	BD*(1)C21-S24	38.41	0.29	0.098
LP(1)N22	BD*(2)C19-N23	23.00	0.28	0.074
	BD*(1)C21-S24	71.58	0.23	0.116
LP(1)N23	BD*(1)C19-O20	8.76	0.76	0.073
	BD*(1)C21-N22	6.80	0.87	0.069
LP(1)S 24	BD*(1)O20-C21	3.69	0.97	0.055
	BD*(1)C21-N22	5.16	1.12	0.069
LP(2)S24	BD*(1)O20-C21	20.17	0.47	0.088
	BD*(1)C21-N22	11.94	0.62	0.078
LP (2)Cl 26	BD*(1)C13-C 14	4.2	0.88	0.054
LP(3)Cl26	BD*(2)C13-C14	12.89	0.32	0.063

^a $E^{(2)}$ means energy of hyperconjugative interactions.

^b Energy difference between donor and acceptor i and j NBO orbitals.

^c $F(i, j)$ is the Fock matrix element between i and j NBO orbitals.

Highlights

- Synthesis and spectral characterization of new oxadiazole derivative are presented
- The compound exists as thione-(T2) tautomer rather than thiol-(T1) one.
- The calculated NMR spectra of T2 correlated well with the experimental data than T1
- The NBO analysis is used to explain the intramolecular charge transfer interactions

Graphical Abstract

Experimental and Theoretical Spectroscopic Studies, HOMO–LUMO, NBO Analyses and Thione-Thiol Tautomerism of a New Hybrid of 1,3,4-Oxadiazole-thione with Quinazolin-4-one

Saied M. Soliman, Mohamed Hagar, Farahate Ibid, El Sayed H. El Ashry*

Optimized molecular structure and molecular electrostatic potential (MEP) calculated at B3LYP/6-311G++(d,p) method of hybrid 3-(4-chlorophenyl)-2-[(5-thioxo-4,5-dihydro-1,3,4-oxadiazol-2-yl)methylthio]quinazolin-4(3H)-one **2**

